RSC Advances

PAPER

View Article Online
View Journal | View Issue

Cite this: *RSC Adv.*, 2023, **13**, 4641

Quantum modeling of dimethoxyl-indaceno dithiophene based acceptors for the development of semiconducting acceptors with outstanding photovoltaic potential

Ehsan Ullah Rashid,[a] N. M. A. Hadia,[*b] Ahmed M. Shawky,[*c] Nashra Ijaz,[a] Manel Essid,[df] Javed Iqbal,[*a] Naifa S. Alatawi,[e] Muhammad Ans[*a] and Rasheed Ahmad Khera[*a]

In the current DFT study, seven dimethoxyl-indaceno dithiophene based semiconducting acceptor molecules (**ID1–ID7**) are designed computationally by modifying the parent molecule (**IDR**). Here, based on a DFT exploration at a carefully selected level of theory, we have compiled a list of the optoelectronic properties of **ID1–ID7** and **IDR**. In light of these results, all newly designed molecules, except **ID5** have shown a bathochromic shift in their highest absorbance (λ_{max}). **ID1–ID4**, **ID6** and **ID7** molecules have smaller band gap (E_{gap}) and excitation energy (E_x). IP of **ID5** is the smallest and EA of **ID1** is the largest among all others. Compared to the parent molecule, **ID1–ID3** have increased electron mobility, with **ID1** being the most improved in hole mobility. **ID4** had the best light harvesting efficiency in this investigation, due to its strongest oscillator. The acceptor molecules' open-circuit voltages (V_{OC}) were computed after being linked to the PTB7-Th donor molecule. Fill factor (FF) and normalized V_{OC} of **ID1–ID7** were calculated and compared to the parent molecule. Based on the outcomes of this study, the modified acceptors may be further scrutinised for empirical usage in the production of organic solar cells with enhanced photovoltaic capabilities.

Received 13th December 2022
Accepted 18th January 2023

DOI: 10.1039/d2ra07957g

rsc.li/rsc-advances

1. Introduction

Solar energy is amongst the most prospective forms of green and sustainable energy and a photovoltaic cell is a device that transforms the unending sun's supply into electricity. Commercially available silicon (Si) solar cells have an extraordinary power conversion efficiency (PCE), but their manufacture is energy-intensive and pollutes the environment significantly due to the processing and purifying of silicon crystals.[1–3] In contrast, organic solar cells (OSCs) of the third generation have the benefits of a simplified device fabrication, inexpensive solution preparation, and the potential to be produced as bendable and semitransparent systems.[4–7] The PCE of OSCs has amplified rapidly because of the recent developments in the engineering and manufacturing of highly efficient optoelectronic semiconductors and improvement on the device fabrication.[8–13] In particular, n-type organic semiconductor (n-OS) based small acceptor molecules[14–17] with a low bandgap (E_{gap}), when combined with a p-type donor polymer having a medium E_{gap}, have shown remarkable optoelectronic performance.[18–20] The PCE of polymer based solar cells having an n-OS as an accepting moiety has increased to a 14%, surpassing the limit for PSCs to be used in practical settings.[21–23] The majority of highly efficient donor and acceptor optoelectronic materials, though, currently contain complex chemical geometries.[24,25] Large amounts of energy are required, and a substantial expense is incurred, during their manufacture due to the many purifications and poor yields that are inevitable.

Presently, ITIC[26] and IDIC[27] are the two most popular and commonly utilized examples of highly efficient n-OS acceptors. The maximum absorption (λ_{max}) of ITIC is 664 nm in dichloromethane, while the compound shows considerable absorption from 500 to 750 nm. The ITIC film has an optical bandgap of 1.59 eV, while its electron mobility may reach to 3.0×10^{-4} cm^2 V^{-1} s^{-1}.[26] Contrarily, λ_{max} of IDIC is seen about 640 nm, with substantial absorption observed between 500 and

[a]*Department of Chemistry, University of Agriculture, Faisalabad 38000, Pakistan. E-mail: javedkhattak79@gmail.com; javed.iqbal@uaf.edu.pk; ansbhatti24@gmail.com; rasheedahmadkhera@yahoo.com; rasheed.ahmad.khera@uaf.edu.pk*

[b]*Physics Department, College of Science, Jouf University, P.O. Box 2014, Sakaka, Al-Jouf, Saudi Arabia. E-mail: nmhadia@ju.edu.sa*

[c]*Science and Technology Unit (STU), Umm Al-Qura University, Makkah 21955, Saudi Arabia*

[d]*Chemistry Department, College of Science, King Khalid University (KKU), P.O. Box 9004, Abha, Saudi Arabia*

[e]*Physics Department, Faculty of Science, University of Tabuk, Tabuk 71421, Saudi Arabia. E-mail: nsalatawi@ut.edu.sa*

[f]*Université de Carthage, Faculté des Sciences de Bizerte, LR13ES08 Laboratoire de Chimie des Matériaux, Zarzouna Bizerte, 7021, Tunisia*

800 nm dichloromethane solution (10^{-6} M). The optical bandgap of IDIC is 1.60 eV, and its electron mobility is very high *i.e.*, 1.1 × 10^{-3} cm^2 V^{-1} s^{-1}.[27,28] Though when blended with PDCBT-Cl, its maximum output voltage (0.94 V) and fill factor (64.2%) values are slightly lower to the ITIC (1.01 V and 64.8%), but its PCE of 9.12% is quite higher to the 7.05% of ITIC, which could be due to its higher short circuit current value of 15.0 mA cm^{-2} compared to the 10.6 mA cm^{-2} of its counterpart.[29] In contrast to ITIC, IDIC has alkyl side groups on its IDT centre, a small fused ring in its central entity, and so has the capability to be the least priced acceptor. Furthermore, the stated technique for the production of ITIC requires a difficult multiple steps procedure with tedious post-production,[30] *e.g.* the Wolff–Kishner reduction reaction and Friedel–Crafts acylation reaction. As a consequence, the productivity is poor, and the costing is expensive. In contrast, the alkylation of ring-closure employed in IDIC synthesizing process may have a poor yield of the core fused-ring group because of the adverse reaction of alkyl chain dehydration. A more effective strategy for preparing the n-OS acceptors with alkyl side-groups was, hence, required.

Amberlyst15, a catalyst employed in the synthesis of IDIC's core fused ring, was described by Li *et al.* as a means of simplifying and optimizing the synthesis process, with potential cost savings for the final product.[31] Following this, they generated a fused-ring entity MO-IDT and enhanced the production of the core fused-ring component by adding alkoxy (–OR) groups to it. Using MO-IDT as a building block, the inexpensive acceptor MO-IDIC was synthesized, and its photovoltaic characteristics were studied in depth. The observed absorption spectra revealed that MO-IDIC have a potential absorption of 600–700 nm along with a maximum absorption at 670 nm. There was a significant PCE increase (11.16%) in PTQ10-donor MO-IDIC-acceptor PSCs. According to the findings, MO-IDIC shows promise as a low-priced n-OS acceptor for potential PSC applications in the future.[31]

In the present research, we have used MO-IDIC as a reference molecule (**IDR**) and have replaced lengthy alkyl chains with methyl groups, for the sake of saving time and effort, because the existence of long alkyl chains do not impose any considerable impact on the optoelectronic features of the molecules.[32,33] The electron donor core of **IDR** is dimethoxyl-indaceno dithiophene based and 2-(2-methylene-3-oxo-indan-1-ylidene)-malononitrile is the end-group (EG) existing on the both peripheral sites of the core. Seven new acceptors (**ID1–ID7**) have been developed computationally by replacing the exiting EGs of **IDR** with 1-dicyanomethylene-2-methylene-3-oxo-indan-5,6-dicarbonitrile in **ID1**, 1-dicyanomethylene-2-methylene-3-oxo-indan-5,6-dicarboxylic acid dimethyl ester in **ID2**, 6-cyano-1-dicyanomethylene-2-methylene-3-oxo-indan-5-carboxylic acid methyl ester in **ID3**, 2-(3-chloro-5-methylene-6-oxo-5,6-dihydrocyclopenta[*c*]thiophen-4-ylidene)-malononitrile in **ID4**, 5,6-difluoro-2-methylene-3-(2,2,2-trifluoro-1-trifluoromethyl-ethylidene)-indan-1-one in **ID5**, 5,6-dichloro-3-dinitromethylene-2-methylene-indan-1-one in **ID6**, and (5,6-difluoro-2-methylene-3-oxo-indan-1-ylidene)-methanedisulfonic acid in **ID7** correspondingly, as shown in Fig. 1.

2. Computational aspects

The Gaussian 09 software[34] was used for all required computations. The molecules, including the reference, were devised using the GaussView 6.0.16.[35] For the purpose of **IDR** optimization, density functional theory (DFT) computations are done run using 6-31G(d,p) basis set with B3LYP,[36] CAM-B3LYP,[37] MPW1PW91,[38] and wB97XD[39] functionals. After **IDR**'s structure was optimized, we used time-dependent DFT simulations to predict its light-absorbing characteristics. We investigated the effect of the solvent (chloroform) on these characteristics using the IEFPCM approach.[40] The theoretical technique was validated by contrasting the theoretically predicted maximum absorption (λ_{max}) of **IDR** from the preceding four functionals to empirically observed λ_{max} data from the research. A comparison is made between the empirical max of **IDR** (670 nm)[31] and the four predicted λ_{max} *i.e.* 656 nm, 624 nm, 519 nm, and 537 nm (Fig. 2). To get the best appropriate findings for the computationally created compounds, we found that simulations using the B3LYP functional were the most closest in accord with the empirical observations.

Origin 6.0 was used to generate the profiles of the compounds' absorption.[41] We studied the transition density matrix (TDM) and utilized Multiwfn[42] to examine the paths and interactions of excitons. PyMOlyze 1.1 (ref. 43) was used in order to produce graphs illustrating the density of states (DOS).[44] In order to compute the intramolecular and intermolecular mobility of charges, the Marcus theory has been used, and the reorganization energy (RE) was investigated.[45,46] However, intramolecular charge transfer (ICT) is what we focused on for this investigation. RE refers to the interplay of two distinct but linked reorganization energies. Exterior RE is affected by intense environmental oscillations and polarity fluctuations that occur while the charge transfer, internal RE is mostly reliant on differences in molecule structure.[47] For this investigation, we can only focus on internal RE since we cannot use external RE to verify our estimations. Using eqn (1) and (2),[48] we calculated the RE for hole (λ_+) and electron (λ_-) mobility.

$$\lambda_+ = [E_+{}^0 - E_0] + [E_0{}^+ - E_+] \quad (1)$$

$$\lambda_- = [E_-{}^0 - E_0] + [E_0{}^- - E_-] \quad (2)$$

$E_+{}^0$ and $E_-{}^0$ signifies the neutral energies of the molecules generated from the optimal form of cation and anions. Anion and cation energies, $E_0{}^-$ and $E_0{}^+$ are calculated from the ground state optimization of the neutral molecule. Computed anion and cation energy estimated from the respective anion and cation optimized geometry. E_0 is the energy of a molecule's neutrally optimized ground state.[49]

3. Results and discussion

3.1. Optimization of geometries

DFT-based optimization of the molecular geometry derives directly the electronic probability density, which can then be used to compute the system's energy.[50] In this work, the studied

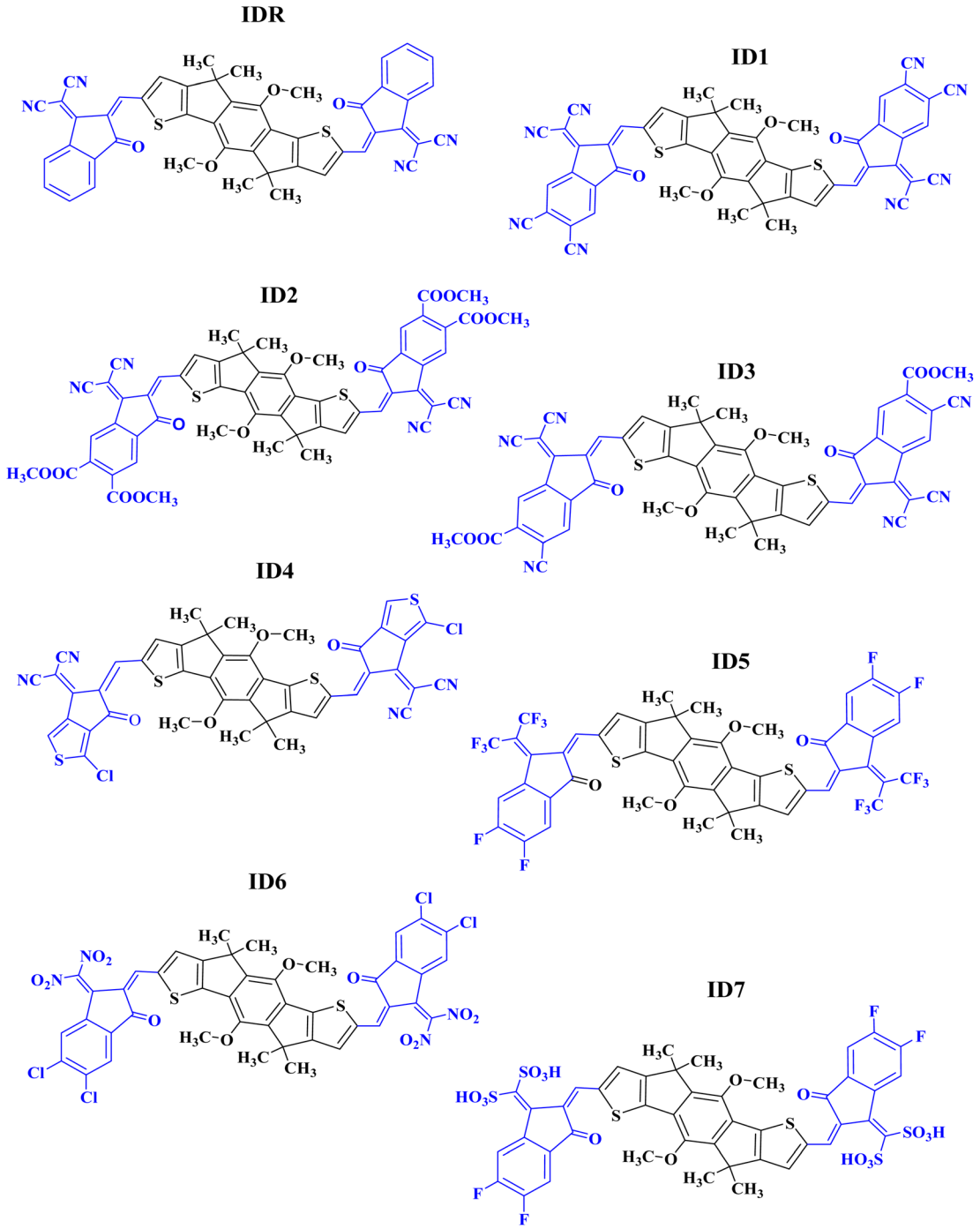

Fig. 1 ChemDraw structures of IDR and ID1–ID7.

molecules, have been optimized using a DFT-based functional *i.e.* B3LYP.[36] The optoelectronic characteristics are very sensitive to the molecule geometry.[51] Fig. 3 demonstrates that both the benchmark (**IDR**) and the newly produced compounds (**ID1–ID7**) were optimized using the selected DFT functional. The continuous transfer of π-electrons enables charge transmission in these materials exceedingly robust, and the molecules' broad conjugation, which covers the complete molecule from core to peripherals, allows for effective charge transfer. By measuring the dihedral angles ($\theta°$)[52] and bond lengths (L_{C-C})[53] of **IDR** as well as **ID1–ID7** molecules, we may infer their degree of planarity and conjugation (see Table 1). Double bonds (C=C) between carbon atoms have a distance of 1.34 Å, whereas single bonds (C–C) have a distance of 1.54 Å. Each of the suggested compounds (**ID1–ID7**) has enhanced charge transport qualities and allows for the conjugation enabling delocalization of electrons due to a L_{C-C} between 1.41 and 1.42 Å, in contrast to IDR, which has an L_{C-C} of 1.49 Å. The $\theta°$ values for all compounds

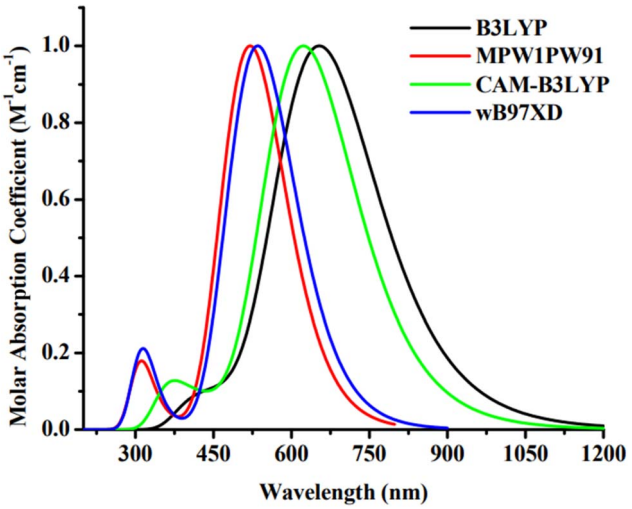

Fig. 2 Absorption plot of IDR using four distinct functionals.

ranged from 0.32° to 4.74°. By this logic, we know that the EGs of any given molecule lie flat against its core.

3.2. Frontier molecular orbitals (FMOs)

It is critical to examine the FMOs since doing so exposes how well the molecules facilitate charge transit and electric potential dispersion.[54] It aids in understanding how charge is transferred and promoted around OSCs. Conduction mechanism, absorptivity, and other electrical characteristics of molecules are dramatically affected by their HOMO and LUMO energies. When discussing OSCs and other photovoltaic processes, it is important to note the presence of the energy gap (E_{gap}), which reflects the proportion of energy needed for the excitation of electrons.[55] It is seen that molecules with low band gap generally produce low values of open-circuit voltage, but absorb greater sunlight and thus produces increased amount of current, and *vice versa*. So, the band gap should be in an optimal range for the molecule to generate effective photovoltaic attributes of all the studied parameters.[56] Extremely polarizable, fragile reaction kinetics, and highly reactive molecules have a low E_{gap}.[57] The calculated FMOs and E_{gap} energies of the **IDR** and **ID1–ID7** molecules are analyzed to estimate the effect of several electron accepting EGs on the photochemical aspects of the molecules under consideration (Table 2). Fig. 4 displays the HOMO and LUMO energies, as well as the E_{gap}, for each molecule.

Most of a molecule's charge in its ground state is found in its core region, which is called the donor region. The EG accepting subunits are the most peripheral parts of a molecule that receive charges when the molecule is in an excited state. The planarity of molecular structures allow for significant charge transport functions, and charge mobility features of compounds from donor to acceptor locations is proof of this effective conjugation. The **IDR** compound has a HOMO, LUMO, and E_{gap} of −5.68, −3.44, and 2.24 eV. The **ID1** molecule has the highly-stable HOMO of all the compounds tested, with a value of −6.25 eV for its HOMO. **ID1**'s electrostatic potential dispersion, which has made the ground-state extremely stable, is most likely due to electron-withdrawing cyano groups in the molecule's EG units. **ID3** possesses highly-stable HOMO after **ID1**, and its comparatively low HOMO of −6.08 eV is the reason for this. The electronegative ester and cyano groups in the EG of **ID3** is the most probable reason behind its second stables HOMO. The declining patterns of examined compounds' HOMO and LUMO orbiting energy values are **ID5** > **IDR** > **ID4** > **ID2** > **ID7** > **ID6** > **ID3** > **ID1** and **ID5** > **IDR** > **ID4** > **ID2** > **ID7** > **ID6** > **ID3** > **ID1**, respectively. The E_{gap} of every recently proposed molecule has decreased as compared to **IDR** molecule, with the exception of **ID5**. As a result of the strong electronegative EGs, the E_{gap} is shrunk, which improves the molecule's charge transfer capacities. **ID5** > **IDR** > **ID7** > **ID2** > **ID3** = **ID4** > **ID1** > **ID6** is the declining trend of E_{gap} for all studied compounds.

3.3. Electron affinity (EA) and ionization potential (IP)

The efficiency of transfer of charges might be influenced by various aspects, including IP and EA. EA is the released energy after addition of any electron to a molecule, while IP is the needed energy for an electron removal.[58] When the both these factors of a molecule are high, it means that it has highly stable HOMO, which makes removing electrons from it more difficult and electrons can be efficiently released from molecules with low IPs and EAs. Strong IP and EA of compounds are the result of electron-withdrawing components that stabilize the HOMO state while compounds with low IP and EA are brought on by HOMO destabilizing electron-donor components.[59] Eqn (3) and (4)[60] are used to calculate both these parameters.

$$\mathrm{IP} = [E_0^{+} - E_0] \quad (3)$$

$$\mathrm{EA} = [E_0 - E_0^{-}] \quad (4)$$

Table 2 lists the calculated IP and EA of **IDR** and **ID1–ID7** molecules. The largest IP (7.74 eV) and EA (3.37 eV) of any other investigated molecule are found in **ID1**, which has a highly stable HOMO (−6.25 eV). The most HOMO-destabilized molecule, **ID5**, has the lowest IP (6.25 eV) and EA (2.31 eV) of all the molecules.

3.4. Optical properties

The light absorbance spectrum can be used to infer the electronic characteristics of the chromophore with great precision. Table 3 enlisted the approximated optical characteristics of **IDR** and **ID1–ID7** in chloroform. The absorption of **IDR** and **ID1–ID7** starts from 300 to 1200 nm in chloroform solvent (Fig. 5). Except **ID5**, all newly designed molecules have bathochromic shift in their λ_{max}. **IDR** and **ID5** have λ_{max} peaks at 654 nm and 607 nm, respectively. λ_{max} of **ID1–ID4**, **ID6** and **ID7** molecules are 702 nm, 673 nm, 685 nm, 673 nm, 725 nm and 675 nm, respectively. The λ_{max} of **ID1–ID4**, **ID6**, and **ID7** compounds shifted from the **IDR** by 19 nm to 71 nm in the UV-visible spectrum, demonstrating a bathochromic behaviour in $CHCl_3$ solvent. Planar molecular structure facilitates stronger conjugation, which in turn increases

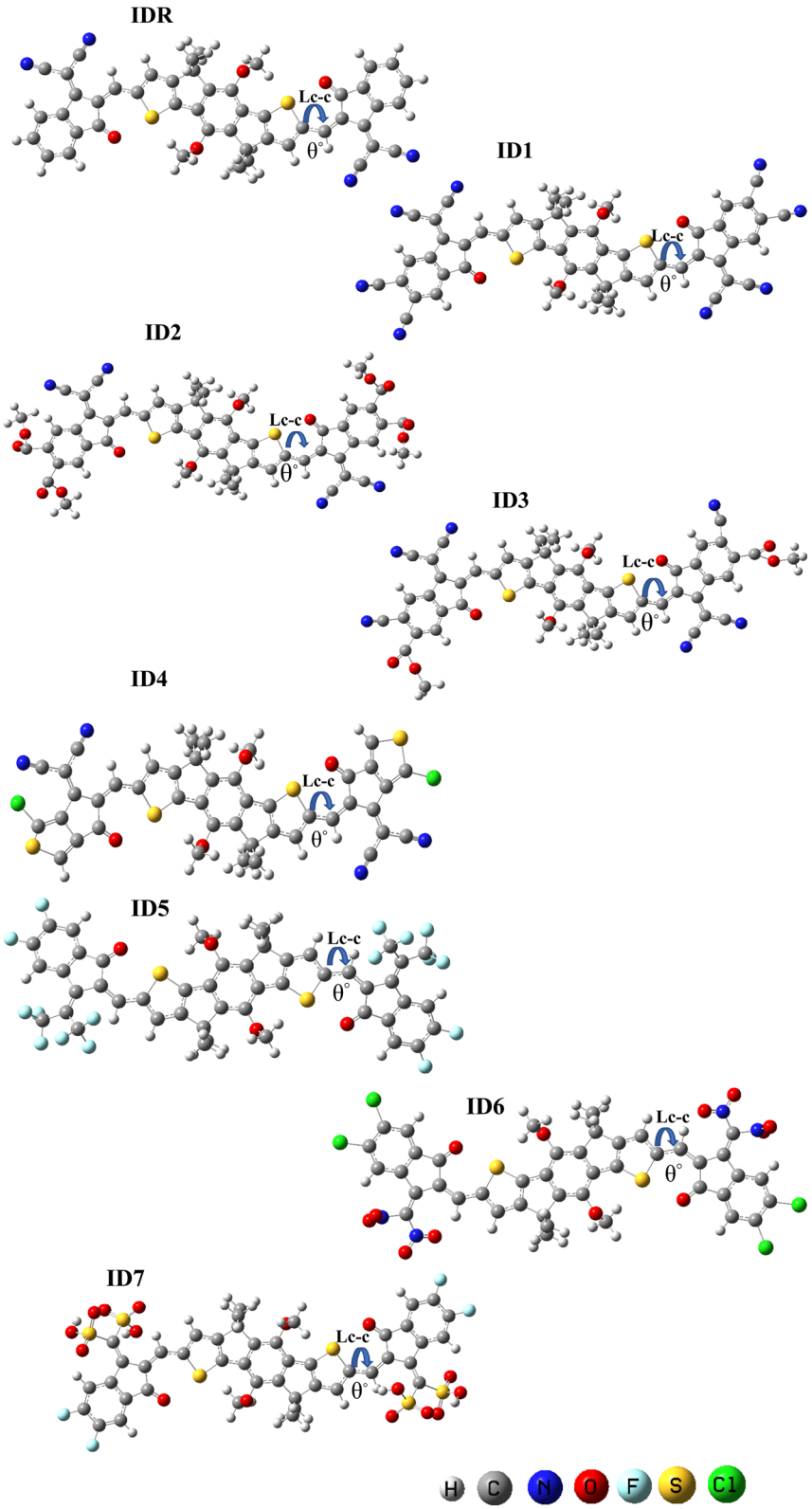

Fig. 3 The optimized geometry of IDR and ID1–ID7 using B3LYP/6-31G(d,p) level.

optical absorption.[61] All the compounds with the smallest E_{gap} also had the longer wavelengths, since the relationship between the two is inverse. The examined compounds' rising λ_{max} trends in the $CHCl_3$ solvent are shown by **ID5** < **IDR** < **ID2** = **ID4** < **ID7** < **ID3** < **ID1** < **ID6**. In $CHCl_3$ solvent, the findings demonstrate that **ID6** has the highest max at 725 nm. This is ascribed to the pair of

Table 1 Computed geometry parameters of IDR and ID1–ID7

Molecules	Bond length (Å)	Dihedral angle (θ°)
IDR	1.49	0.32
ID1	1.41	0.68
ID2	1.42	0.65
ID3	1.42	0.69
ID4	1.42	2.52
ID5	1.42	4.74
ID6	1.41	1.83
ID7	1.41	2.36

Table 2 HOMO level, LUMO level, E_{gap}, electron affinity (EA) and ionization potential (IP) of IDR and ID1–ID7 in eV

Molecules	HOMO	LUMO	E_{gap}	IP	EA
IDR	−5.68	−3.44	2.24	6.53	2.66
ID1	−6.25	−4.14	2.11	7.74	3.37
ID2	−5.82	−3.62	2.19	6.53	2.77
ID3	−6.08	−3.92	2.16	6.80	3.18
ID4	−5.75	−3.59	2.16	6.53	2.82
ID5	−5.60	−3.23	2.37	6.25	2.31
ID6	−5.96	−3.87	2.09	6.80	3.02
ID7	−5.95	−3.72	2.23	6.80	2.85

electronegative chloro and nitro groups in the EG acceptors of **ID6** molecule.

There is a non-dimensional variable called the oscillator strength (f) that has a profound effect on the optical characteristics of OSC systems and the strength of the radiation emitted by electric stimulation throughout the energy state.[62] Potential changes need a certain amount of energy, known as excitation energy (E_x).[63] Moreover, increasing f, reducing E_x, or broadening the absorbance range may all enhance ICT. Newly suggested molecules, with the exception of **ID5**, all have lower E_x values as opposed to **IDR**.

Each component of a solar cell, has to be capable to produce an electric current after exposure to light which often called light-harvesting efficiency.[64] LHE has an impact on how well the system absorbs energy, and oscillator strength has an impact as well because of how much short-circuit current (J_{SC}) it produces. Eqn (5) was used to estimate the LHE for each compound examined.

$$\mathrm{LHE} = 1 - 10^{-f} \quad (5)$$

Table 3 lists the LHE values determined for the **IDR** and **ID1–ID7** molecules in $CHCl_3$ solvent. Overall, the LHE values for **ID2** and **ID4** molecules were greater than **IDR**. Since **ID4** has a stronger oscillation strength, it yields the most LHE. The LHE of **ID3** is the same as the LHE of **IDR**, while **ID5** is nearly equal to the LHE of **IDR**. The lower LHE of the remaining molecules might be because of the negative influence of their end groups on the transition probability, leading to reduced oscillator strength and LHE values. Specifically, the LHE values of all, except for **ID1** and **ID6**, are higher or comparative to the reference molecule.

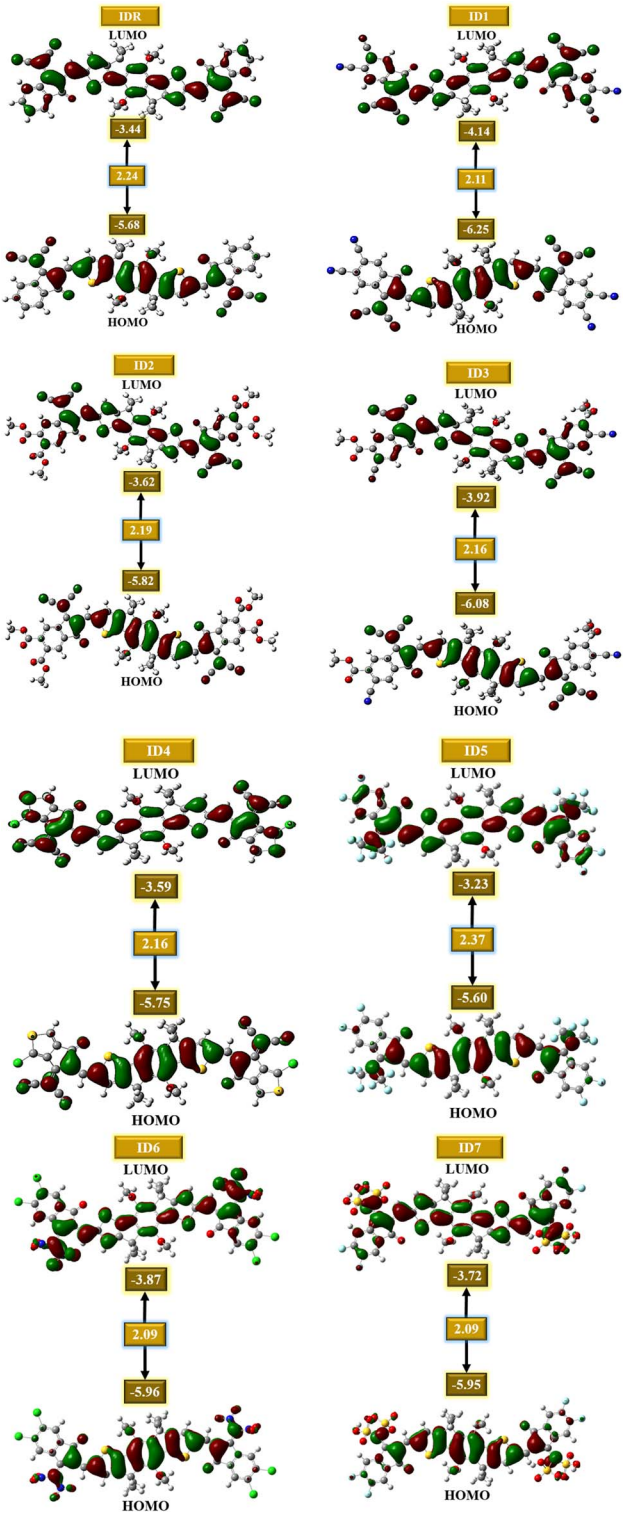

Fig. 4 FMOs of IDR and ID1–ID7.

3.5. Dipole moment (D)

When determining the solubility and crystalline phase, the dipole moment (D) is crucial. Such characteristics are crucial in defining polarizing behaviours in the solvent desired for efficient organic photovoltaic systems.[65] Charge may be

Table 3 Computed λ_{max}, E_x, LHE, oscillator strength (f), and transition character of IDR as well as ID1–ID7 compounds in $CHCl_3$

Molecules	Experimental λ_{max} (nm)	Computed λ_{max} (nm)	E_x (eV)	f	LHE	Transition character (H → L) (%)
IDR	670	654	1.89	2.54	0.9971	70
ID1	—	702	1.76	2.36	0.9956	70
ID2	—	673	1.84	2.57	0.9973	70
ID3	—	685	1.81	2.53	0.9971	70
ID4	—	673	1.84	2.63	0.9976	70
ID5	—	607	2.03	2.52	0.9970	70
ID6	—	725	1.70	2.05	0.9912	70
ID7	—	675	1.83	2.51	0.9969	70

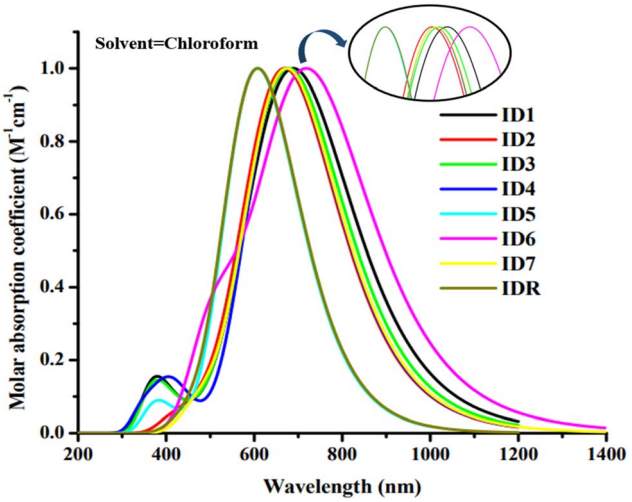

Fig. 5 Absorption spectra of IDR and ID1–ID7 molecules.

transported regularly in compounds with a high D value because of their planar and ordered shape. As a consequence, the crystalline character of the compound is enhanced, and it becomes more soluble in polar-solvents due to the tight packing of its structural components. Higher D numbers indicate that molecules are more prone to crystallize, and that they disperse more easily in polar liquids, both of which enhance charge transmission.[66] Molecules with negligible D value are often not soluble in polar aprotic solvents like $CHCl_3$. This correlation is not, however, always true since the molecular structure of a given molecule determines its reactivity toward solvents and its ability to transmit charges.[63] Table 4 exhibit numerical data indicating an escalating order of D for molecules *i.e.* **IDR** < **ID6** < **ID1** < **ID5** < **ID7** < **ID2** < **ID4** < **ID3** and **IDR** < **ID1** < **ID6** < **ID5** < **ID7** < **ID2** < **ID4** < **ID3** studied in both stages (gas and $CHCl_3$ respectively). **ID1–ID7** have much higher D values than **IDR**, which improves their solubility and crystallinity. The occurrence of cyano and ester moieties at the EGs are the reason why ID3 possesses the highest D value.

3.6. Density of states (DOS)

Studies of DOS are essential for learning how the various elements (donor, acceptor, *etc.*) of a compound work together. The corresponding DOS that can be both partial and total, determines the entire capability of molecules.[67] When planning the placement of FMOs in respect to the Mulliken charge density, DOS estimation is a crucial first step. At the designated level of theory, the DOS was deliberated for all of the probed molecules and PyMOlyze 1.1 was used to generate charts and graphs from the data. In the generated plots, the x-axis represents energy, while y-axis signifies relative intensity. Peaks depicting HOMO energy may be seen out to the left of the graphs' central line (the E_{gap}). However, the peaks that represent LUMO energy may be seen to the right of the centre line. Separating each molecule into its donor and acceptor pieces allowed us to analyse the effect of each individual unit on the FMOs.

In the DOS schemes of **IDR** and **ID1–ID4** and **ID7** molecules, red and green lines show the donor and acceptor contribution in the FMOs and in **ID5** and **ID6** molecules, red and green lines are showing the contribution of acceptor–donor subunits in the FMOs (Fig. 6). Table 5 provides quantitative measure of inputs from each components. It is expected from the outcomes that the core donor component has a more significant role in the HOMO state, whereas acceptor component plays a greater role in the LUMO state in all of the tested compounds' FMOs. This offers irrefutable confirmation for the feasibility of charge transfer by successive conjugation between donor and acceptor components of a molecule, which has the capability to increase the ultimate efficacy of OSCs. From Fig. 4, it can be concluded that these observations agree with the FMOs of the investigated compounds. Because of their planar shape, molecules are able to effectively transport charge from electron-rich donor core area to the peripheral electron-accepting EGs in excited state, as shown by the results.

Table 4 Dipole moment of IDR as well as ID1–ID7 in both stages of gas and $CHCl_3$, respectively

Molecules	D (gas phase)	D (solvent phase)
IDR	0.00022	0.000283
ID1	0.40909	0.005511
ID2	3.06192	3.658809
ID3	6.83557	7.914996
ID4	4.49408	5.449057
ID5	1.12053	1.289791
ID6	0.00627	0.007537
ID7	2.89507	3.557854

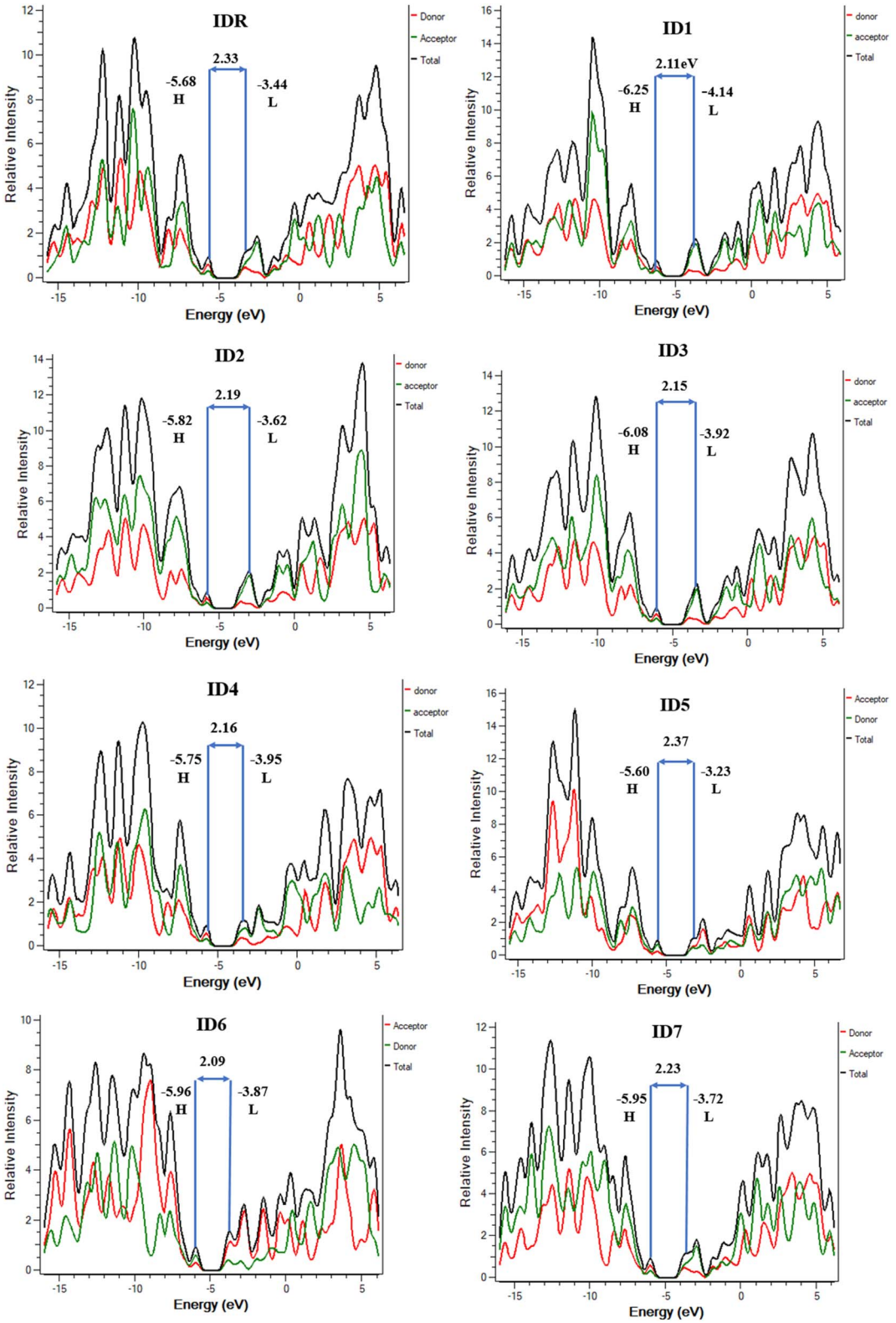

Fig. 6 DOS plots of IDR and ID1–ID7 molecules.

3.7. Reorganization energy (RE)

RE of **ID1–ID7** and **IDR** molecules was measured to examine the charge transfer between charge accepting and donating subunits. The RE offers a quantified estimate of the charges moved from molecule's donor section to the acceptor, and is therefore connected to mobility of electrons and holes of the

Table 5 Acceptor and donor subunits involvement in the FMOs of studied molecules

Molecules	FMOs	Acceptor (%)	Donor (%)
IDR	HOMO	34.8	65.2
	LUMO	53.9	46.1
ID1	HOMO	37.0	63.0
	LUMO	66.9	33.1
ID2	HOMO	35.7	64.3
	LUMO	63.9	36.1
ID3	HOMO	36.4	63.6
	LUMO	64.4	35.6
ID4	HOMO	36.4	63.6
	LUMO	64.4	35.6
ID5	HOMO	26.6	73.4
	LUMO	52.8	47.2
ID6	HOMO	34.9	65.1
	LUMO	64.8	35.2
ID7	HOMO	36.0	64.0
	LUMO	53.5	46.5

molecule, making it the most crucial factor in the design of components that are useful for OSCs.[68] Actually, the RE is inversely correlated to the electrons and holes' mobility. For this reason, by decreasing the RE, charge transmission efficiency is improved.[69] Anion and cation geometry formations are only one of many potential factors that might influence RE. Table 6 displays the results of calculating the RE of hole and electron for each molecule under study with eqn (1) and (2). The studies imply that the augmented molecular mix attributable to the plane geometries of some of the newly suggested molecules is responsible for the higher hole and electron mobility recorded for those molecules.

ID1–ID3, with their lower RE of λ_- (0.1469, 0.1061 and 0.1850 eV), have higher electron mobility than **IDR** (0.1986 eV). The resulting molecular mix has a finer morphology because of the plane geometric models, which boost exciton dispersion and electron mobility. Since **ID2** exhibited the lowest RE for electron mobility (0.1061 eV) among the molecules studied, this finding suggests that the EGs recently grafted onto the molecule had a significant impact in improving its electron transport properties. **ID2** < **ID1** < **ID3** < **IDR** < **ID4** < **ID6** < **ID5** < **ID7** is the examined compounds' λ_- sequence. Remarkably, **ID1** (0.1687 eV) has the greatest hole mobility of all the studied molecules since its RE for hole mobility has decreased the most.

Table 6 RE of electron (λ_-) and hole (λ_+) for IDR and ID1–ID7

Molecule	λ_- (eV)	λ_+ (eV)
IDR	0.1986	0.1741
ID1	0.1469	0.1687
ID2	0.1061	0.1904
ID3	0.1850	0.1986
ID4	0.2067	0.1768
ID5	0.3346	0.2231
ID6	0.3237	0.2176
ID7	0.4299	0.3428

3.8. Electrostatic potential (ESP)

ESP signifies presence as well as absence of electrons, along with the 3D distribution of charges outside of a molecule.[70] To forecast which reacting sites are present somewhere in a molecule's framework, we used the ESP approach to the substances that we had studied in great detail. The ESP maps display the three-dimensional distribution of lone pair, unbounded-electrons, and electron-rich components that are amenable to nucleophilic reactivity. ESP diagrams include dark red spots representing regions of high electron density around oxygen and nitrogen atoms at the EGs of molecules (Fig. 7). Because oxygen is present at EGs, its characteristic red hue serves as an indicator of the high electron density present across these spots. However, oxygen is present in the centre of molecules displaying blue and green hues, and the electrons deficient carbon atoms nearby cancels out the electrostatic concentration of the oxygen there.[46] On the ESP maps, methyl and benzene and thiophene rings are shaded blue to indicate a significant deficiency of electrons.

3.9. Transition density matrix (TDM) and exciton binding energy (E_b)

TDM assessment is essential for precisely predicting the exciton flux in between electron accepting and donating units in conjugated geometries at particular sites.[71] It is feasible to predict charges transmissions, major charge patches, and the position of exciton motions throughout emissions and absorbance in the excited state by the use of this technique.[72] TDM plots are created in order to examine electronic features, such as the degree of delocalization and the influence of resonance, as well as to understand how charges travel inside molecules. Hydrogen is often disregarded in TDM research because of the concept that its impact on electrostatic interaction is negligible. On the *y*-axis and *x*-axes, atoms that of molecules with no hydrogen in it are present. The coefficient representing the charge potential is displayed by the bar towards the right of the plot that has a gradient from blue to red along the *x*-axis. The electrostatic frequency can be seen in acceptor (A) and donor (D) both areas of **IDR** and **ID1–ID7** (Fig. 8). Electrostatic potential alternates between flowing diagonally and off-diagonally from donor to acceptor all throughout the molecule, with the former being the more prevalent of the two. The images displayed the sequential conjugation of the compounds' EGs with the donor core sections, demonstrating the systematic transmission of electric densities from the donor central segment to the EGs.

E_b is also important since it may be utilized as a predictor for the exciton (electron–hole) segregation possibilities, OSC functioning, and electrical qualities.[73] Analysing the interaction among electron–hole pairs depending on coulombic forces yields the quantity of E_b.[74] Electron–hole coulombic interaction is weak if E_b is small, and *vice versa*. According to this analysis's eqn (6), the projected values for E_b are shown in Table 7.

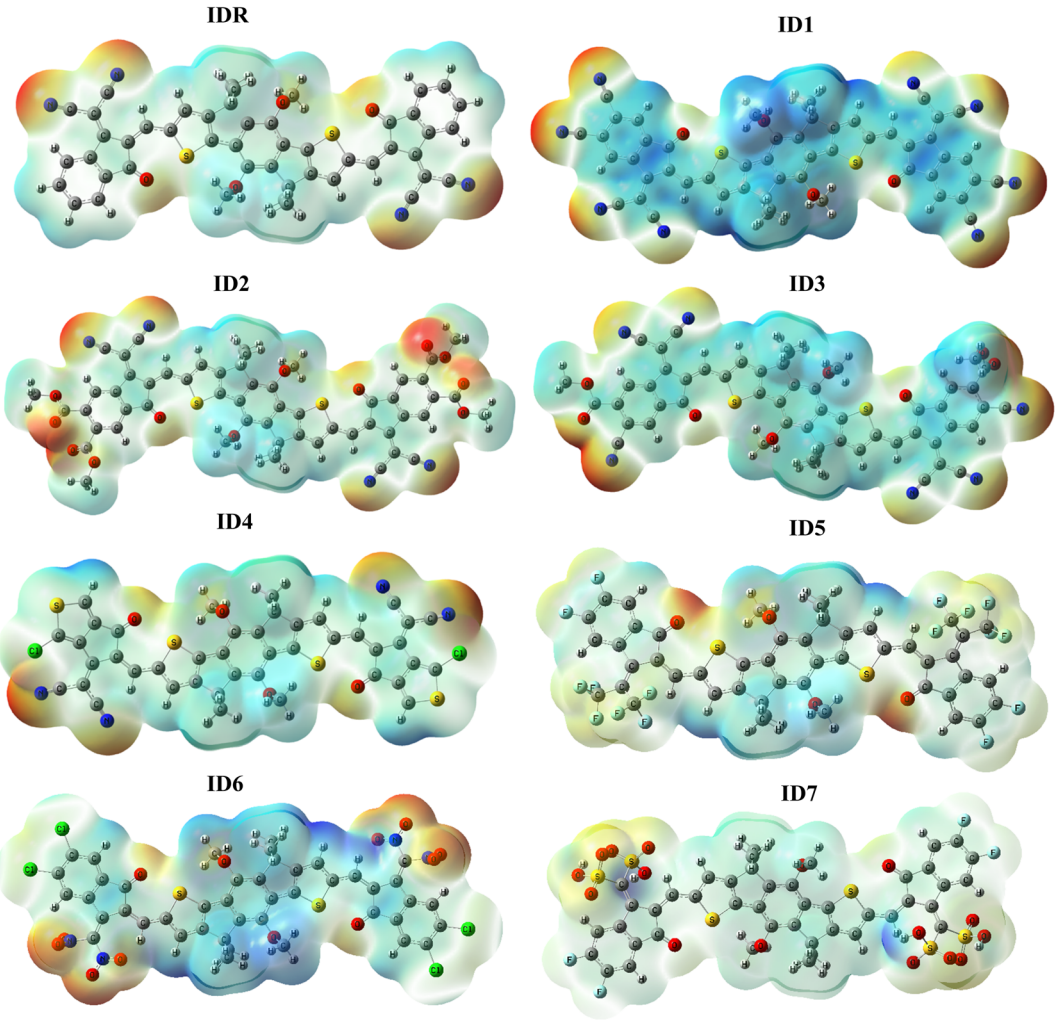

Fig. 7 ESP plots of IDR and ID1–ID7 molecules.

$$E_b = E_{gap} - E_x \quad (6)$$

We observe that the E_b values of **ID1** and **ID5** are virtually equal to those of **IDR**. **ID4** has the lowest E_b (0.32 eV) in the $CHCl_3$ solvent as compared to other investigated molecules.

3.10. Performance of device

Any solar instrument's photovoltaic aptitude can be assessed by quantifying its open circuit voltage (V_{OC}), making it a key aspect of understanding how the device functions.[75] When no additional current is placed on an optical device, the voltage measured as V_{OC} indicates the maximum voltage that can be delivered by the device.[76] The highest voltage is generated when the HOMO from donor compound and LUMO from acceptor one are linked together. Reduced HOMO energies of donor and the increased LUMO energies of the acceptor are required to achieve the increased V_{OC} values. In the presented work, the HOMO of PTB7-Th donor was coupled with studied acceptors' LUMO (**IDR, ID1–ID7**) to release the utmost V_{OC}. The available study demonstrates that PTB7-Th, with its HOMO and LUMO energy of −5.20 and −3.60 eV, is a reliable donor for theoretical calculations due to its comparable LUMO value to the NFAs' LUMO for easy charge transfer.[77] Here, we used eqn (7)[78] to get a numerical approximation of V_{OC} values.

$$V_{OC} = \frac{E^{LUMO}_{ACCEPTOR} - E^{HOMO}_{DONOR}}{e} - 0.3 \quad (7)$$

The e is the charge symbol for molecules, has a value of 1. The coefficient of charge between surfaces, often about 0.30. The proposed small acceptors (**IDR, ID1–ID7**) and PTB7-Th donor are shown in Fig. 9 together with their estimated V_{OC} and FMOs. Evidence suggests that **ID5** molecules have a higher V_{OC} value (1.67 eV) than **IDR** molecules do (1.46 eV). The ascending V_{OC} order of all newly proposed is **ID1** < **ID3** < **ID6** < **ID7** < **ID2** < **ID4** < **ID5** (Table 8). Findings showed that **ID5** had the greatest V_{OC} value, indicating the possibility that it may be utilized in efficient OSC.

The fill factor (FF) is an essential factor in determining the PV system's PCE. The V_{OC} present at the interface of the

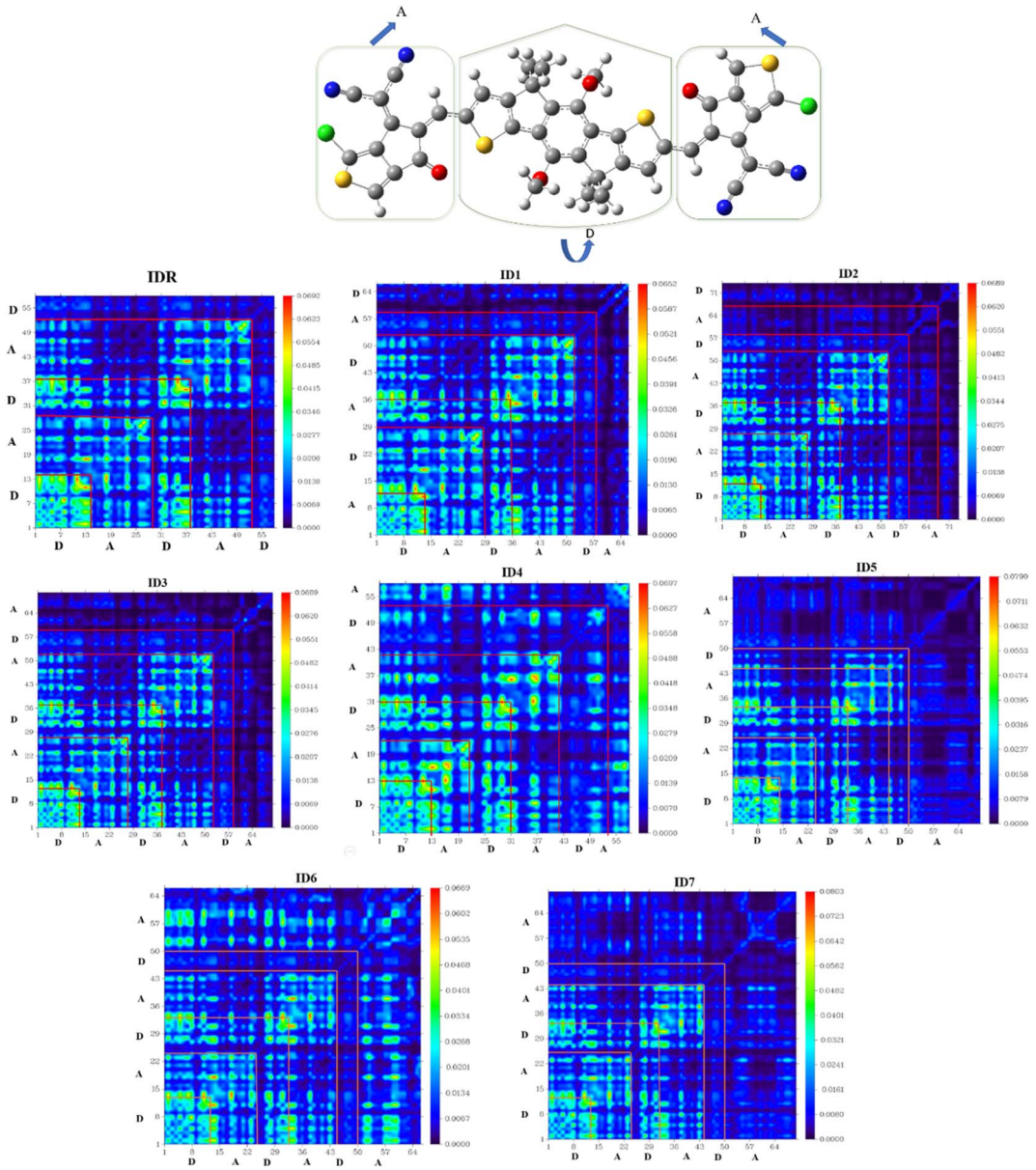

Fig. 8 TDM plots of **IDR** and **ID1–ID7** molecules.

Table 7 E_{gap}, excitation energy (E_x), and exciton binding energy (E_b) of **IDR** and **ID1–ID7** in eV

Molecule	E_{gap}	E_x	E_b
IDR	2.24	1.89	0.34
ID1	2.11	1.76	0.34
ID2	2.19	1.84	0.35
ID3	2.16	1.81	0.35
ID4	2.16	1.84	0.32
ID5	2.37	2.03	0.34
ID6	2.09	1.70	0.39
ID7	2.23	1.83	0.40

acceptor–donor materials has a major impact on FF. The FF of all the compounds in our investigation were determined using the following formula (8).[79]

$$FF = \frac{\frac{eV_{OC}}{K_B T} - \ln\left(\frac{eV_{OC}}{K_B T} + 0.72\right)}{\frac{eV_{OC}}{K_B T} + 1} \quad (8)$$

In eqn (8), $\frac{eV_{OC}}{K_B T}$ is the normalized V_{OC}. Where e is average charge with a value of 1. K_B is the Boltzmann constant and T is temperature of 300 K. The final findings show that compared to the original molecule, **ID5** has better normalized V_{OC} and FF (64.59 and 0.9210) as compared to the **IDR** molecule (56.47 and

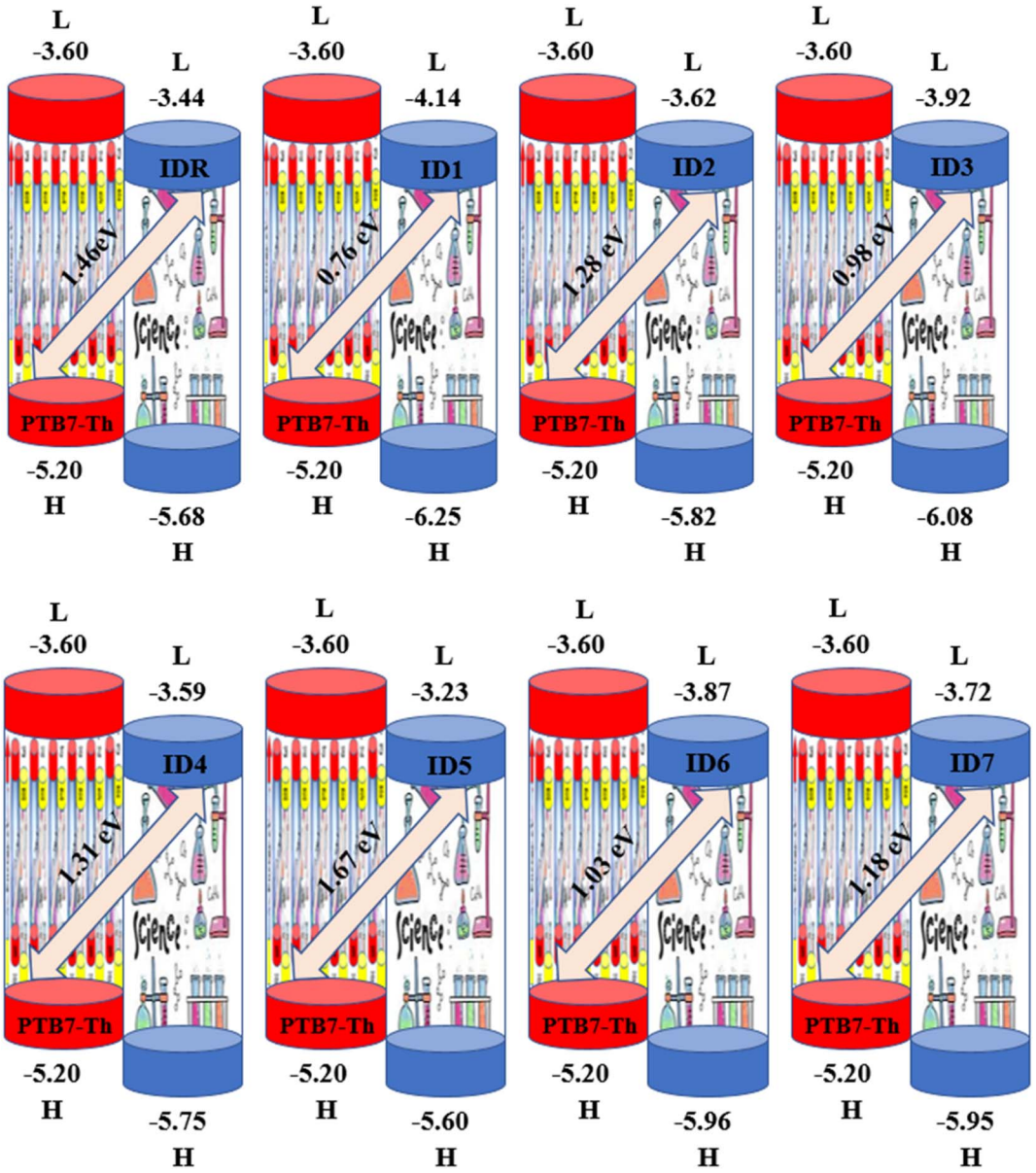

Fig. 9 V_{OC} of IDR and ID1–ID7 acceptors with PTB7-Th donor.

Table 8 V_{OC}, normalized V_{OC} and FF of IDR and ID1–ID7

Molecule	V_{OC} (eV)	Normalized V_{OC} $\left(\frac{eV_{OC}}{K_B T}\right)$	Fill factor
IDR	1.46	56.47	0.9121
ID1	0.76	29.39	0.8550
ID2	1.28	49.51	0.9026
ID3	0.98	37.90	0.8803
ID4	1.31	50.67	0.9045
ID5	1.67	64.59	0.9210
ID6	1.03	39.84	0.8848
ID7	1.18	45.64	0.8963

0.9121), respectively (Table 8). On a side note, the FF values of the molecules, as studied computationally, are much higher than the possible experimental ones. However, they give an appropriate estimate and helps in determination of the molecules with higher experimental FF (though lower than the theoretical one) than other molecules.

PCE is calculated to see whether the PV substance is adequately effective for usage in practical systems and it compiles the relevant parameters of solar equipment's functioning into a single number.[80] The PCE of a molecule is majorly influenced by the V_{OC}, FF, and J_{SC}. One of the best representations of this connection is given by eqn (9).

$$\mathrm{PCE} = \frac{J_{SC} V_{OC} \mathrm{FF}}{P_{in}} \quad (9)$$

Using the aforementioned formulae, this study computationally calculates the V_{OC} and FF for the molecules **IDR** and **ID1–ID7**; however, the J_{SC} was not computed owing to limited

capabilities. It has been shown previously how LHE is one of the variables used to calculate the J_{SC}. The newly created molecule in this study, **ID5**, has been shown to have higher PCE than **IDR**, as expected by the increased V_{OC} and FF.

4. Conclusion

In this study, seven small acceptor-molecules (**ID1–ID7**) were computationally designed to optimize OSC performance by modifying the reference molecule's (**IDR**) EG acceptor. Our calculations of the new compounds' optoelectronic properties, using the B3LYP/6-31G(d,p) level of theory, are equated to those of the original molecule. The E_{gap} of every recently proposed molecule has decreased (2.11–2.23 eV) as opposed to **IDR** (2.24 eV), with the exception of **ID5** (2.37 eV). The **ID1** has the largest EA (3.37 eV) and **ID5** possesses the smallest IP (6.25 eV) in this study. Except **ID5**, all newly designed molecules have bathochromic shift in their λ_{max}. The λ_{max} of **ID1–ID4**, **ID6** and **ID7** molecules are 702 nm, 673 nm, 685 nm, 673 nm, 725 nm and 675 nm, respectively. LHE of **ID2** and **ID4** molecules were better than **IDR**. **ID1–ID7** have much higher dipole moment values than **IDR**, which improves their solubility and crystallinity. **ID1–ID3**, with their lower RE of λ_{-} (0.1469, 0.1061, and 0.1850 eV), have higher electron mobility than **IDR** (0.1986 eV). Remarkably, **ID1** (0.1687 eV) has the greatest hole mobility of all the studied molecules since its RE for hole mobility has decreased the most. In the present work, the HOMO of PTB7-Th donor was coupled with the LUMO of the studied NFAs (**IDR**, **ID1–ID7**) to produce the maximum and **ID5** molecules have a higher V_{OC} value (1.67 eV) than **IDR** molecules do (1.46 eV). These findings suggest that the changed molecules deserve additional research as a means to develop OSC with improved photovoltaic performance.

Conflicts of interest

The authors declare no conflict of interest.

Acknowledgements

The authors acknowledge the technical support from Department of Chemistry University of Agriculture, Faisalabad, Pakistan. The authors from the King Khalid University extend their appreciation to Deanship of Scientific Research at King Khalid University for funding the work through the general research project (GRP-311-43). The authors would like to thank the Deanship of Scientific Research at Umm Al-Qura University for supporting this work by Grant Code: (22UQU4331174DSR51). We also thank Dr Khurshid Ayub, COMSATS University, Islamabad for additional resource.

References

1 Y. Liu, *et al.*, Aggregation and morphology control enables multiple cases of high-efficiency polymer solar cells, *Nat. Commun.*, 2014, **5**(1), 1–8.
2 G. Li, *et al.*, High-efficiency solution processable polymer photovoltaic cells by self-organization of polymer blends, *Nat. Mater.*, 2005, **4**(11), 864–868.
3 G. Li, R. Zhu and Y. Yang, Polymer solar cells, *Nat. Photonics*, 2012, **6**(3), 153–161.
4 C. J. Traverse, *et al.*, Emergence of highly transparent photovoltaics for distributed applications, *Nat. Energy*, 2017, **2**(11), 849–860.
5 Q. Tai and F. Yan, Emerging semitransparent solar cells: materials and device design, *Adv. Mater.*, 2017, **29**(34), 1700192.
6 Y. Li, Molecular Design of Photovoltaic Materials for Polymer Solar Cells: Toward Suitable Electronic Energy Levels and Broad Absorption, *Acc. Chem. Res.*, 2012, **45**(5), 723–733.
7 R. Søndergaard, *et al.*, Roll-to-roll fabrication of polymer solar cells, *Mater. Today*, 2012, **15**(1–2), 36–49.
8 L. Ye, *et al.*, Surpassing 10% efficiency benchmark for nonfullerene organic solar cells by scalable coating in air from single nonhalogenated solvent, *Adv. Mater.*, 2018, **30**(8), 1705485.
9 P. Cheng, *et al.*, Ternary system with controlled structure: a new strategy toward efficient organic photovoltaics, *Adv. Mater.*, 2018, **30**(8), 1705243.
10 S. Li, *et al.*, An unfused-core-based nonfullerene acceptor enables high-efficiency organic solar cells with excellent morphological stability at high temperatures, *Adv. Mater.*, 2018, **30**(6), 1705208.
11 E. U. Rashid, *et al.*, Synergistic end-capped engineering on non-fused thiophene ring-based acceptors to enhance the photovoltaic properties of organic solar cells, *RSC Adv.*, 2022, **12**(20), 12321–12334.
12 M. Li, *et al.*, Solution-processed organic tandem solar cells with power conversion efficiencies > 12%, *Nat. Photonics*, 2017, **11**(2), 85–90.
13 X. Che, *et al.*, High fabrication yield organic tandem photovoltaics combining vacuum-and solution-processed subcells with 15% efficiency, *Nat. Energy*, 2018, **3**(5), 422–427.
14 Y. Zhou, *et al.*, High efficiency small molecular acceptors based on novel O-functionalized ladder-type dipyran building block, *Nano Energy*, 2018, **45**, 10–20.
15 G. Zhang, *et al.*, Efficient nonfullerene polymer solar cells enabled by a novel wide bandgap small molecular acceptor, *Adv. Mater.*, 2017, **29**(18), 1606054.
16 J. Hou, *et al.*, Organic solar cells based on non-fullerene acceptors, *Nat. Mater.*, 2018, **17**(2), 119–128.
17 Z. Yao, *et al.*, Dithienopicenocarbazole-based acceptors for efficient organic solar cells with optoelectronic response over 1000 nm and an extremely low energy loss, *J. Am. Chem. Soc.*, 2018, **140**(6), 2054–2057.
18 J.-S. Wu, *et al.*, Donor–acceptor conjugated polymers based on multifused ladder-type arenes for organic solar cells, *Chem. Soc. Rev.*, 2015, **44**(5), 1113–1154.
19 H. Yao, *et al.*, Molecular design of benzodithiophene-based organic photovoltaic materials, *Chem. Rev.*, 2016, **116**(12), 7397–7457.

20 G. Y. Ge, *et al.*, Unveiling the Interplay among End Group, Molecular Packing, Doping Level, and Charge Transport in N-Doped Small-Molecule Organic Semiconductors, *Adv. Funct. Mater.*, 2022, **32**(7), 2108289.
21 J. Sun, *et al.*, Dithieno[3,2-b:2′,3′-d]pyrrol fused nonfullerene acceptors enabling over 13% efficiency for organic solar cells, *Adv. Mater.*, 2018, **30**(16), 1707150.
22 S. Zhang, *et al.*, Over 14% efficiency in polymer solar cells enabled by a chlorinated polymer donor, *Adv. Mater.*, 2018, **30**(20), 1800868.
23 Z. Fei, *et al.*, An alkylated indacenodithieno[3,2-b] thiophene-based nonfullerene acceptor with high crystallinity exhibiting single junction solar cell efficiencies greater than 13% with low voltage losses, *Adv. Mater.*, 2018, **30**(8), 1705209.
24 S. j. Xu, *et al.*, A Twisted Thieno[3,4-b]thiophene-Based Electron Acceptor Featuring a 14-π-Electron Indenoindene Core for High-Performance Organic Photovoltaics, *Adv. Mater.*, 2017, **29**(43), 1704510.
25 H. Bin, *et al.*, 11.4% Efficiency non-fullerene polymer solar cells with trialkylsilyl substituted 2D-conjugated polymer as donor, *Nat. Commun.*, 2016, **7**(1), 1–11.
26 Y. Lin, *et al.*, An electron acceptor challenging fullerenes for efficient polymer solar cells, *Adv. Mater.*, 2015, **27**(7), 1170–1174.
27 Y. Lin, *et al.*, A facile planar fused-ring electron acceptor for as-cast polymer solar cells with 8.71% efficiency, *J. Am. Chem. Soc.*, 2016, **138**(9), 2973–2976.
28 B. Guo, *et al.*, High efficiency nonfullerene polymer solar cells with thick active layer and large area, *Adv. Mater.*, 2017, **29**(36), 1702291.
29 Z. Liang, *et al.*, Optimization requirements of efficient polythiophene: nonfullerene organic solar cells, *Joule*, 2020, **4**(6), 1278–1295.
30 L. Cai, *et al.*, 4,9-Dihydro-4,4,9,9-tetrahexyl-s-indaceno[1,2-b:5,6-b′]dithiophene as a π-spacer of donor–π–acceptor dye and its photovoltaic performance with liquid and solid-state dye-sensitized solar cells, *Org. Lett.*, 2014, **16**(1), 106–109.
31 X. Li, *et al.*, Simplified synthetic routes for low cost and high photovoltaic performance n-type organic semiconductor acceptors, *Nat. Commun.*, 2019, **10**(1), 1–11.
32 E. U. Rashid, *et al.*, Engineering of W-shaped benzodithiophenedione-based small molecular acceptors with improved optoelectronic properties for high efficiency organic solar cells, *RSC Adv.*, 2022, **12**(34), 21801–21820.
33 K. Lin, *et al.*, Star-shaped electron acceptors containing a truxene core for non-fullerene solar cells, *Org. Electron.*, 2018, **52**, 42–50.
34 M. Frisch, *et al.*, *Gaussian 09, revision D.01*, Gaussian, Inc., Wallingford, CT, 2009.
35 R. Dennington, T. A. Keith and J. M. Millam, *GaussView, version 6.0.16*, Semichem Inc., Shawnee Mission, KS, 2016.
36 B. Civalleri, *et al.*, B3LYP augmented with an empirical dispersion term (B3LYP-D*) as applied to molecular crystals, *CrystEngComm*, 2008, **10**(4), 405–410.
37 T. Yanai, D. P. Tew and N. C. Handy, A new hybrid exchange–correlation functional using the Coulomb-attenuating method (CAM-B3LYP), *Chem. Phys. Lett.*, 2004, **393**(1–3), 51–57.
38 C. Adamo and V. Barone, Exchange functionals with improved long-range behavior and adiabatic connection methods without adjustable parameters: the mPW and mPW1PW models, *J. Chem. Phys.*, 1998, **108**(2), 664–675.
39 J.-D. Chai and M. Head-Gordon, Long-range corrected hybrid density functionals with damped atom–atom dispersion corrections, *Phys. Chem. Chem. Phys.*, 2008, **10**(44), 6615–6620.
40 J. Tomasi, B. Mennucci and R. Cammi, Quantum mechanical continuum solvation models, *Chem. Rev.*, 2005, **105**(8), 2999–3094.
41 L. Deschenes and A. David, *Origin 6.0: Scientific Data Analysis and Graphing Software Origin Lab Corporation (Formerly Microcal Software, Inc.)*, Vanden Bout University of Texas, 2000, p. 595, **www.originlab.com**.
42 T. Lu and F. Chen, Multiwfn: a multifunctional wavefunction analyzer, *J. Comput. Chem.*, 2012, **33**(5), 580–592.
43 A. L. Tenderholt, *PyMOlyze: A Program to Analyze Quantum Chemistry Calculations*, 2019.
44 S. Alexander and R. Orbach, Density of states on fractals: "fractons", *J. Phys., Lett.*, 1982, **43**(17), 625–631.
45 Z. Shuai, *et al.*, Applying Marcus theory to describe the carrier transports in organic semiconductors: limitations and beyond, *J. Chem. Phys.*, 2020, **153**(8), 080902.
46 E. U. Rashid, *et al.*, Depicting the role of end-capped acceptors to amplify the photovoltaic properties of benzothiadiazole core-based molecules for high-performance organic solar cell applications, *Comput. Theor. Chem.*, 2022, **1211**, 113669.
47 G. R. Hutchison, M. A. Ratner and T. J. Marks, Hopping transport in conductive heterocyclic oligomers: reorganization energies and substituent effects, *J. Am. Chem. Soc.*, 2005, **127**(7), 2339–2350.
48 M. U. Saeed, *et al.*, Structural modification on dimethoxythienothiophene based non-fullerene acceptor molecule for construction of high-performance organic chromophores by employing DFT approach, *J. Phys. Chem. Solids*, 2022, **170**, 110906.
49 E. U. Rashid, *et al.*, Quantum chemical modification of indaceno dithiophene-based small acceptor molecules with enhanced photovoltaic aspects for highly efficient organic solar cells, *RSC Adv.*, 2022, **12**(44), 28608–28622.
50 I. N. Levine, D. H. Busch and H. Shull, *Quantum chemistry*, Pearson Prentice Hall, Upper Saddle River, NJ, 2009, vol. 6.
51 J. Zhou, *et al.*, Small molecules based on benzo[1,2-b:4,5-b′] dithiophene unit for high-performance solution-processed organic solar cells, *J. Am. Chem. Soc.*, 2012, **134**(39), 16345–16351.
52 A. Altis, *et al.*, Dihedral angle principal component analysis of molecular dynamics simulations, *J. Chem. Phys.*, 2007, **126**(24), 244111.

53 S. Yang and M. Kertesz, Bond length alternation and energy band gap of polyyne, *J. Phys. Chem. A*, 2006, **110**(31), 9771–9774.
54 M. Ans, J. Iqbal, Z. Ahmad, S. Muhammad, R. Hussain, B. Eliasson and K. Ayub, Designing three-dimensional (3D) non-fullerene small molecule acceptors with efficient photovoltaic parameters, *ChemistrySelect*, 2018, **3**(45), 12797–12804.
55 M. Salim, *et al.*, Amplifying the photovoltaic properties of azaBODIPY core based small molecules by terminal acceptors modification for high performance organic solar cells: a DFT approach, *Sol. Energy*, 2022, **233**, 31–45.
56 B. R. Sutherland, Solar materials find their band gap, *Joule*, 2020, **4**(5), 984–985.
57 U. Azeem, *et al.*, Tuning of a A–A–D–A–A-Type Small Molecule with Benzodithiophene as a Central Core with Efficient Photovoltaic Properties for Organic Solar Cells, *ACS Omega*, 2021, **6**(43), 28923–28935.
58 J. Widmer, *et al.*, Open-circuit voltage and effective gap of organic solar cells, *Adv. Funct. Mater.*, 2013, **23**(46), 5814–5821.
59 A. Farhat, *et al.*, Tuning the optoelectronic properties of subphthalocyanine (SubPc) derivatives for photovoltaic applications, *Opt. Mater.*, 2020, **107**, 110154.
60 E. U. Rashid, *et al.*, Quantum chemical modification of indaceno dithiophene-based small acceptor molecules with enhanced photovoltaic aspects for highly efficient organic solar cells, *RSC Adv.*, 2022, **12**(44), 28608–28622.
61 I. Zubair, *et al.*, Tuning the optoelectronic properties of indacenodithiophene based derivatives for efficient photovoltaic applications: a DFT approach, *Chem. Phys. Lett.*, 2022, **793**, 139459.
62 M. U. Saeed, *et al.*, End-capped modification of Y-shaped dithienothiophen[3,2-b]-pyrrolobenzothiadiazole (TPBT) based non-fullerene acceptors for high performance organic solar cells by using DFT approach, *Surf. Interfaces*, 2022, **30**, 101875.
63 M. Rafiq, *et al.*, End-capped modification of dithienosilole based small donor molecules for high performance organic solar cells using DFT approach, *J. Mol. Liq.*, 2022, **345**, 118138.
64 M. Ans, *et al.*, Designing alkoxy-induced based high performance near infrared sensitive small molecule acceptors for organic solar cells, *J. Mol. Liq.*, 2020, **305**, 112829.
65 A. Sharif, *et al.*, Tuning the optoelectronic properties of dibenzochrysene (DBC) based small molecules for organic solar cells, *Mater. Sci. Semicond. Process.*, 2021, **127**, 105689.
66 M. Rani, *et al.*, Strategies toward the end-group modifications of indacenodithiophene based non-fullerene small molecule acceptor to improve the efficiency of organic solar cells; a DFT study, *Comput. Theor. Chem.*, 2022, 113747.
67 M. Waqas, *et al.*, Impact of end-capped modification of MO-IDT based non-fullerene small molecule acceptors to improve the photovoltaic properties of organic solar cells, *J. Mol. Graphics Modell.*, 2022, **116**, 108255.
68 M. R. Aslam, *et al.*, Tuning of diphenylamine subphthalocyanine based small molecules with efficient photovoltaic parameters for organic solar cells, *J. Mol. Graphics Modell.*, 2022, **112**, 108146.
69 N. E. Gruhn, *et al.*, The vibrational reorganization energy in pentacene: molecular influences on charge transport, *J. Am. Chem. Soc.*, 2002, **124**(27), 7918–7919.
70 H. Yao, *et al.*, 14.7% efficiency organic photovoltaic cells enabled by active materials with a large electrostatic potential difference, *J. Am. Chem. Soc.*, 2019, **141**(19), 7743–7750.
71 P. Å. Malmqvist, Calculation of transition density matrices by nonunitary orbital transformations, *Int. J. Quantum Chem.*, 1986, **30**(4), 479–494.
72 A. Luzanov, A. Sukhorukov and V. Umanskii, Application of transition density matrix for analysis of excited states, *Theor. Exp. Chem.*, 1976, **10**(4), 354–361.
73 P. Gong, *et al.*, Ultrafast Kinetics Investigation of a Fluorinated-Benzothiadiazole Polymer with an Increased Excited State Transition Dipole Moment Applied in Organic Solar Cells, *ACS Appl. Energy Mater.*, 2021, **4**(9), 9627–9638.
74 Y. A. Duan, *et al.*, Theoretical characterization and design of small molecule donor material containing naphthodithiophene central unit for efficient organic solar cells, *J. Comput. Chem.*, 2013, **34**(19), 1611–1619.
75 A. Rasool, *et al.*, Bithieno Thiophene-Based Small Molecules for Application as Donor Materials for Organic Solar Cells and Hole Transport Materials for Perovskite Solar Cells, *ACS Omega*, 2021, **7**(1), 844–862.
76 I. Zubair, *et al.*, Designing the optoelectronic properties of BODIPY and their photovoltaic applications for high performance of organic solar cells by using computational approach, *Mater. Sci. Semicond. Process.*, 2022, **148**, 106812.
77 J. Sun, *et al.*, High performance non-fullerene polymer solar cells based on PTB7-Th as the electron donor with 10.42% efficiency, *J. Mater. Chem. A*, 2018, **6**(6), 2549–2554.
78 M. C. Scharber, *et al.*, Design rules for donors in bulk-heterojunction solar cells—towards 10% energy-conversion efficiency, *Adv. Mater.*, 2006, **18**(6), 789–794.
79 J. D. Chen, *et al.*, Single-junction polymer solar cells exceeding 10% power conversion efficiency, *Adv. Mater.*, 2015, **27**(6), 1035–1041.
80 R. Rajeswari, *et al.*, Recent progress and emerging applications of rare earth doped phosphor materials for dye-sensitized and perovskite solar cells: a review, *Chem. Rec.*, 2020, **20**(2), 65–88.